CNRS
Centre Nationale de la Recherche Scientifique

INFN
Istituto Nazionale di Fisica Nucleare

A proposal for the VIRGO Detection Bench Positioning Control

(Draft 6 December 1996)

D. Castellazzi
(*castel@virgoa1.in2p3.fr*)

Laboratoire d'Annecy-le-Vieux de Physique des Particules
Chemin de Bellevue BP 110, 74941 Annecy-le-Vieux CEDEX, FRANCE

VIR-NOT-LAP-4200-101
Issue: 1
Date : 20 December 1996

VIRGO * A joint CNRS-INFN Project
Project Office: INFN-Sezione di Pisa * Via Livornese, 1291-56010 San Piero a Grado, Pisa.Italy.
Secretariat: Telephone.(39) 50 880 327 or 880 352* FAX.(39) 50 880 350* e-mail virgo@pisa.infn.it

It's studied and proposed an active feedback control system for the detection bench. It consists of eight magnets-coils couples which act directly on the bench itself from fixed supports attached to the tower floor.

Contents

1 Introduction

We need a positioning control system for the detection bench, that will be ready by 1996, to let us carry out the alignment tests inside the tower. Short time impels us to study a way of controlling the bench directly, so not depending on the last filter stage and on the marionetta control system for the next tests; if it shows satisfactory performances, it would be applied even in the final design.
The advantages of our propose are :

- The simplicity (and so the rapidity) in designing and building it;
- The possibility of reducing, for the moment, the marionetta to a neutral suspending stage, omitting the activators;
- The consequent possibility of suspending the bench and marionetta to a normal stage filter (or straight to the top of the the tower in the tests);

- The absence of contro-reactions and a more direct feedback procedure. We can read the position of the bench and consequently apply the force on the same object, possibly in the same point, from a fixed support, reducing the complications given by the suspension Transfer Function .

The goals of a "bottom-control system" are:

1. Making possible to dump the inevitable bench oscillations in six directions, while it's placed in the right position by displacements of the suspension point (non-linear regime);
2. Performing the feedback forces to control the bench alignment with respect to the beam, in the four required directions (linear regime);
3. Damping the oscillations at the resonant frequencies;

2 Requirements

2.1 Positioning precision

The main alignment constraints on the bench position come from the A-beam matching with the mode-cleaner.
The demanded precisions on the beam position at the mode-cleaner level are [1]:

$$\sigma_{x,y_{mc}} = 4.2 \times 10^{-6} \ m$$
$$\sigma_{\theta,\phi_{mc}} = 73 \times 10^{-6} \ rad$$

We indicate with $\sigma_{x,y}$ an *rms* value of displacement along directions x, y perpendicular to the beam axis z, while $\sigma_{\theta,\phi}$ is referred to rotations around the same axes.
The telescope set in front of it amplifies angular misalignments between bench and beam and reduce the longitudinal ones. The result is a greater sensitivity to angular motion (and consequently more strict limits on such misalignments) than to longitudinal ones.
If we consider the different telescopes that will be used for VIRGO98 and VIRGO2000, we have the demanded precision at the bench entrance:

Bench *rms* displ.	VIRGO98	VIRGO2000
$\sigma_{x,y_{bench}} \leq$	$10^{-4}\ m$	$6.1 \times 10^{-4}\ m$
$\sigma_{\theta,\phi_{bench}} \leq$	$3 \times 10^{-6}\ rad$	$0.5 \times 10^{-6}\ rad$

The bench is not sensitive to rotations around the optical axis z, while is sensitive to movements along it only if greater than few centimeters.
VIRGO will not be sensitive to bench displacements below the *rms* values listed above. So, at first, we should be able to move the bench of amounts bigger than limits given for VIRGO98 to have a usable Positioning Control System. We want to reach the following dynamic ranges, that we consider enough to align the bench with respect to the beam.

$$\boxed{\begin{array}{c}\Delta x, y = 500\ \mu m \\ \Delta\theta, \phi = 5 \times 10^{-3}\ rad\end{array}}$$

[1] *Recherche des ondes gravitationelles avec ...*, A. Dominjon, Doctorate Thesis

2.2 Noise limits

The idea of placing the photodiodes on a separated bench outside the tower is under study. In this case, the external bench would be subjected to seismic noise, so to become a constraint for the noise inserted by the actuators. Moreover, even if the photodiodes will be placed on the internal bench, the seismic noise is an upper rigid limit (otherwise, we wouldn't have reason to suspend the bench).
Horizontal and vertical motions are so modeled by a reference spectrum

$$\tilde{X}_{seis} = \frac{10^{-6}}{\nu^2} \quad \left[\frac{m}{\sqrt{Hz}}\right] \tag{1}$$

above 0.1 Hz and constant below.
Of course, we have verified that this would not be excessive for the alignment requirements at the bench entrance, given by the mode-cleaner:

$$\tilde{x} \ \leq \ 16.7 \times 10^{-6} \ m/\sqrt{Hz} \ \ (@100 \ Hz) \tag{2}$$

Nevertheless, the bench isolation (vibrational and acoustic) is necessary for the strict limit on the variation of the mode cleaner length $\tilde{\delta l} \leq 1.8 \times 10^{-16} \ m/\sqrt{Hz}$ (@100 Hz). An excitation of the bench modes (even if at frequency above 500 Hz) should be coupled with the mode-cleaner modes, in a way at present under study, giving rise to the feared length variation.

Concerning the limits on the angular noise spectral density, we should take the specifications for VIRGO2000 on the beam alignment at the bench entrance @100 Hz, that is surely the most stringent value.

Spectral Noise	@10 Hz	@100 Hz
$\tilde{x}, \tilde{y} \ \leq$	$10^{-8} \ m/\sqrt{Hz}$	$10^{-10} \ m/\sqrt{Hz}$
$\tilde{\theta}, \tilde{\phi} \ \leq$	$1.4 \times 10^{-8} \ rad/\sqrt{Hz}$	$1.4 \times 10^{-8} \ rad/\sqrt{Hz}$

3 Mechanical Characteristics

3.1 Detection Bench

The bench will be worked from an Aluminum monobloc, after thermal stabilization, in octagonal shape; the internal diameter is of 0.88 m, while the external one is of 0.952 m.
Its mass is 36 kg, raised to 50 kg with a cover, so to have its own resonance frequencies at $\sim$ 500 Hz. The mass becomes 60 kg with the optical devices mounted on. The moments of inertia referred to the vertical (x) and horizontal (y, z) axes, are:

$$I_{x_{bench}} = 6.5 \quad Kg \cdot m^2$$
$$I_{yz_{bench}} = 3.3 \quad Kg \cdot m^2$$

It's suspended with 3 wires, of 1 mm diameter and length 0.7 m, to a marionetta of diameter 0.8 m and mass 100 kg and then to a SA with only 2 filtering stages; we take 160 Kg for the total mass of bench+marionetta. The moments of inertia of these two are:

$$I_x = I_{x_{bench}} + I_{x_{mar}} \simeq 14.5 \quad Kg \cdot m^2$$
$$I_{yz} = I_{yz_{bench}} + I_{yz_{mar}} \simeq 7.3 \quad Kg \cdot m^2$$

3.2 Suspension chain

Great importance in our calculations have the resonance frequencies and the elastic constants for the controlled four degrees of freedom. In the case of a simple oscillator they are linked through

$$\nu_{v,h} = \frac{1}{2\pi}\sqrt{\frac{k}{m}} \qquad \nu_{r,t} = \frac{1}{2\pi}\sqrt{\frac{K}{I}} \tag{3}$$

to the constant of force k or to the elastic momentum K.

On the contrary, a bench suspension chain consists of four elements: two seismic filters, the marionetta and the bench itself. The Transfer Function (TF) is calculated by numerical integration of the equations describing the movement, in one dimension, of a chain of massive pendula. It gives us all the informations about resonant frequencies and static displacements when applying a force. Figure (1) shows the vertical and horizontal TF, if applied a force with constant spectrum on the bench.

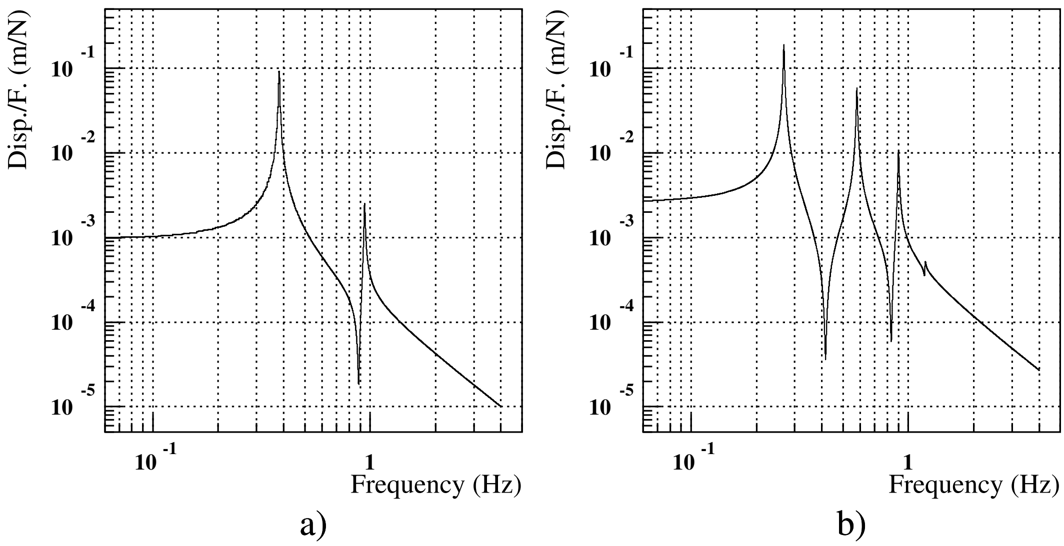

Figure 1: Transfer Function between a force with constant spectrum, applied on the bench, and its displacement: a) Vertical, b) Horizontal.

To evaluate the rotational frequency, we calculate the elastic momentum given by the torsion of the three wires, two suspending the filters (of diameter $d \sim 3\ mm$ and length $l_1 = 2\ m$, $l_2 = 1\ m$), and one suspending the marionetta ($d \sim 2.5\ mm$, $l_3 = 1\ m$) :

$$K_r(l_i, d_i) = \frac{\pi {d_i}^4 Y}{32 l_i} \tag{4}$$

and the momentum of the tension of the three wires suspending the bench, of fixed length, that cause the standing of the bench center of mass during the rotation :

$$K_r' = \frac{mgb^2}{L} \tag{5}$$

with $b = 0.3\ m$, distance of the bench suspension point from the center of it.

The series of these elastic momentum (4),(5) add as:

$$K_r = \left[\sum_i \frac{1}{K_r(l_i, d_i)} + \frac{1}{K'_r} \right]^{-1} = 0.277\ N \cdot m \tag{6}$$

We calculate the tilt restoring momentum given by the flexion of a wire, of diameter d, as:

$$K_t = \frac{1}{16}\sqrt{T\pi d^4 Y} \tag{7}$$

with T tension. For the three wires suspending the bench we obtain $K_t = 4.22\ Nm$, to be summed to the elastic moment from marionetta's wire $K'_t = 10.53\ Nm$. The total result will be:

$$K_t = 14.75\ Nm$$

Finally we can calculate the resonant frequencies. From eq. (3) and Figure (1) we have:

- Rotational: $K_r = 0.277\ Nm$ $\nu_{rot} = 2.2 \times 10^{-2}\ Hz$
- Tilting: $K_t = 14.75\ Nm$ $\nu_{tilt} = 0.23\ Hz$
- Vertical: $k_v = 1017\ N/m$ $\nu_{vert} = 0.38\ Hz$
- Horizontal: $k_h = 369\ N/m$ $\nu_{hor} = 0.27\ Hz$

4 Required Force

We can calculate the needed force and than the coil/magnet dimensions, starting from the wished maximum range of section 2.1.
From Figure (7) at page 15, we can get the geometry of the eight coils. They have been placed on the bench sides at 45° with respect to the beam axis, in order to leave the maximum free space at the bench entrance. The horizontal coils are on the axes of the 45° rotated reference.

The vertical force is obtained through four coils:

$$4 \times F_{max} = k_{vert} \times \Delta x \tag{8}$$

The horizontal force is also obtained through four coils, but placed at 45°:

$$4\frac{\sqrt{2}}{2} \times F_{max} = k_{hor} \times \Delta y \tag{9}$$

Concerning rotations ϕ, we own other four and an arm equal to the bench radius+magnet bracket, $R_r = 495\ mm$:

$$4 \times F_{max} \times R_r = K_{rot} \times \Delta\phi \tag{10}$$

Again, the four coils act for the tilt angle θ, with an arm $R_t = 276\ mm$:

$$4 \times F_{max} \times R_t = K_{tilt} \times \Delta\theta \tag{11}$$

In the table below are summed up the dynamic ranges and the needed force-per-coil to obtain them.

	Ver (x)	Hor (y)	Tilt (θ)	Rot. (ϕ)
Δ	$500\ \mu m$	$500\ \mu m$	$5 \times 10^{-3}\ rad$	$5 \times 10^{-3}\ rad$
F_{coil}	$0.13\ N$	$0.07\ N$	$0.07\ N$	$7 \times 10^{-4}\ N$

5 Magnet-Coil Actuator

5.1 Basic force calculation

Each actuator is composed by one coil of mean radius a and N turns, and a permanent magnet placed along the coil axis and separated from its plane of $a/2$. This arrangement is one-half of a Helmholtz couple. It has been chosen because of its zero force gradient along the axis and its insensitivity to transversal misalignment in a region sufficiently large for our purpose. A Maxwell configuration would show a greater region of constant force, but its arrangement presents mechanical problems (thin magnet support).

The magnetic field produced by the coil, under the hypothesis of negligible section respect to the distance, in a point $P(z,\rho)$ has only two components. The axial one:

$$B_z(z,\rho) = \frac{N\mu_0 IK}{4\pi\sqrt{a\rho}}\left[\frac{a^2-\rho^2-z^2}{(a-\rho)^2+z^2}\cdot J_2(K) + J_1(K)\right] \tag{12}$$

and the radial one:

$$B_\rho(z,\rho) = \frac{N\mu_0 IKz}{4\pi\sqrt{a\rho}}\left[\frac{a^2+\rho^2+z^2}{(a-\rho)^2+z^2}\cdot J_2(K) - J_1(K)\right] \tag{13}$$

with:

$$K = \sqrt{\frac{4a\rho}{(a+\rho)^2+z^2}} \tag{14}$$

and the elliptic Legendre's integrals:

$$J_1(K) = \int_0^{\frac{\pi}{2}} \frac{d\psi}{\sqrt{1-K^2\sin^2\psi}} \qquad J_2(K) = \int_0^{\frac{\pi}{2}} \sqrt{1-K^2\sin^2\psi}\,d\psi \tag{15}$$

The force produced by the interaction with the permanent magnetic moment, z oriented, is:

$$\vec{F} = \vec{\nabla}(\vec{m}\cdot\vec{B}) = m_z\vec{\nabla}B_z \tag{16}$$

which has the same two components of the magnetic field:

$$F_z = m_z\frac{\partial B_z}{\partial z} \tag{17}$$

$$F_\rho = m_z\frac{\partial B_z}{\partial \rho} \tag{18}$$

Along the z axis the radial component of the force vanishes while the axial one take the simpler form:

$$F_z(z,0) = -\frac{3}{2}\frac{\mu_0 NIa^2m_z}{(a^2+z^2)^{5/2}}z \tag{19}$$

that in $z = a/2$ becomes:

$$F_z(\frac{a}{2},0) = -5.4 \cdot 10^{-7} \times m_z \frac{NI}{a^2} \tag{20}$$

useful to get a first estimate of coil's parameters.

5.2 Finite-dimension calculation

In order to evaluate the influence of the coil finite-dimensions on the effective force, we integrated a circular spire field over coil dimensions. Calling L the coil height, and a_e, a_i the external and internal radius, on the coil z axis one can obtain the analytic formula:

$$\begin{aligned} B_z(z,L,a_e,a_i) &= \frac{\mu_0 NI}{2L(a_e-a_i)} \times \left\{ (z+L/2)\ln\left[\frac{a_e+\sqrt{{a_e}^2+(z+L/2)^2}}{a_i+\sqrt{{a_i}^2+(z+L/2)^2}}\right] + \right. \\ & \left. -(z-L/2)\ln\left[\frac{a_e+\sqrt{{a_e}^2+(z-L/2)^2}}{a_i+\sqrt{{a_i}^2+(z-L/2)^2}}\right] \right\} \end{aligned} \tag{21}$$

and than, through eq. (17) :

$$\begin{aligned} F_z(z,m_z,L,a_e,a_i) &= \frac{\mu_0 m_z NI}{2L(a_e-a_i)} \left\{ \ln\left[\frac{a_e+\sqrt{{a_e}^2+(z+L/2)^2}}{a_i+\sqrt{{a_i}^2+(z+L/2)^2}} \cdot \frac{a_i+\sqrt{{a_i}^2+(z-L/2)^2}}{a_e+\sqrt{{a_e}^2+(z-L/2)^2}}\right] + \right. \\ & + \frac{(z+L/2)^2}{\sqrt{{a_e}^2+(z+L/2)^2}\cdot\left(a_e+\sqrt{{a_e}^2+(z+L/2)^2}\right)} + \\ & - \frac{(z+L/2)^2}{\sqrt{{a_i}^2+(z+L/2)^2}\cdot\left(a_i+\sqrt{{a_i}^2+(z+L/2)^2}\right)} + \\ & - \frac{(z-L/2)^2}{\sqrt{{a_e}^2+(z-L/2)^2}\cdot\left(a_e+\sqrt{{a_e}^2+(z-L/2)^2}\right)} + \\ & \left. + \frac{(z-L/2)^2}{\sqrt{{a_i}^2+(z-L/2)^2}\cdot\left(a_i+\sqrt{{a_i}^2+(z-L/2)^2}\right)} \right\} \end{aligned} \tag{22}$$

It's useful to study the F_z dependence from the turns number N. Once fixed the magnet parameters (see Section 5.4), the internal coil diameter d_i and the dissipated power, we can express the other variables I, L, a_e as only function of N.
We take the values:

$$\begin{aligned} m_z &= 0.75\ Am^2 \\ d_i &= 48\ mm \\ P_{max} &= 3\ W \end{aligned}$$

in order to have an internal free space of 42 mm (6 mm of coil's structure thickness, see Fig. 6) and a maximum temperature rise of 9 °C (see Section 5.5).

Besides, from the force expression (22), we can evaluate the mean-force taking in account the longitudinal magnet dimension, $l_z = 12\ mm$, again as function of N:

$$\overline{F_z}(N) = \frac{1}{l_z}\int_{\frac{a}{2}-\frac{l_z}{2}}^{\frac{a}{2}+\frac{l_z}{2}} F_z(N)dz \tag{23}$$

In Figure (2) we plotted the analytic expression (22) of F_z, and $\overline{F_z}$, computed by numerical integration of eq. (23).

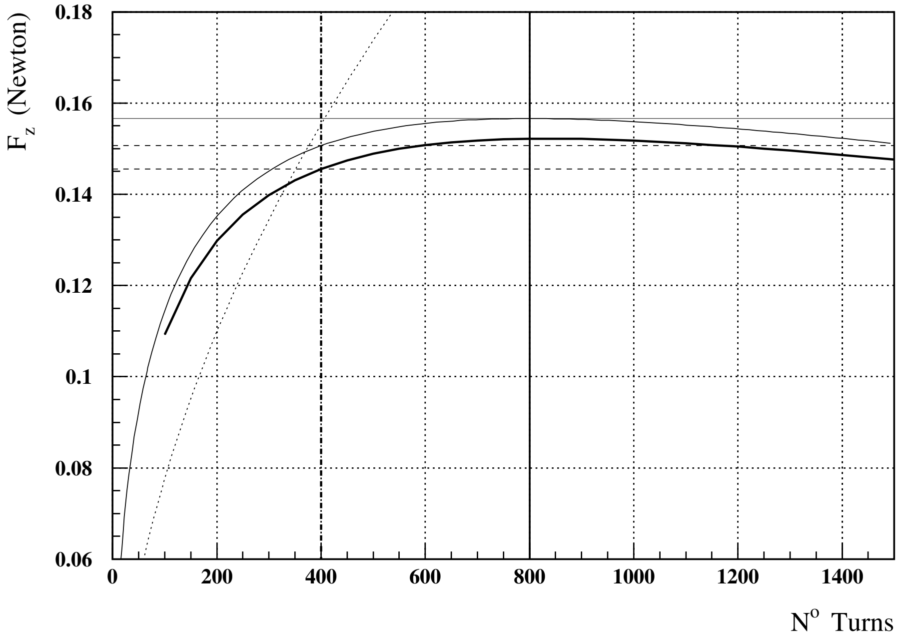

Figure 2: Longitudinal force as function of the turns number. Bold-face line is referred to the mean-force $\overline{F_z}$. Dashed line fixes the selected working point $N = 400$, $F_z(400) = 0.151\ N$, $\overline{F_z}(400) = 0.146\ N$. It's also plotted, with a dotted line, the adimensional calculated force (19), diverging with N.

The turns number $N = 400$ is chosen in order to have a force $\overline{F_z}$ only of 7% smaller than the maximum, obtained at $N = 800$, with the advantage of using half the number of turns. Figures (3) and (4) show the current I, the mean radius a, the overall diameter and the wire length as function of N, after have used the fixed values of m_z, d_i, P written above, to eliminate other variables dependence.

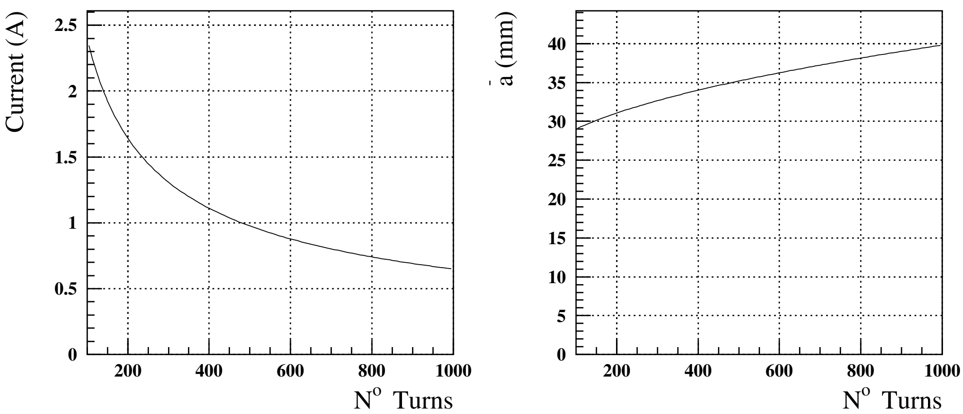

Figure 3: Current and mean radius versus N. The choice $N = 400$ fixes $I = 1.12\ A$ and $\overline{a} = 34\ mm$.

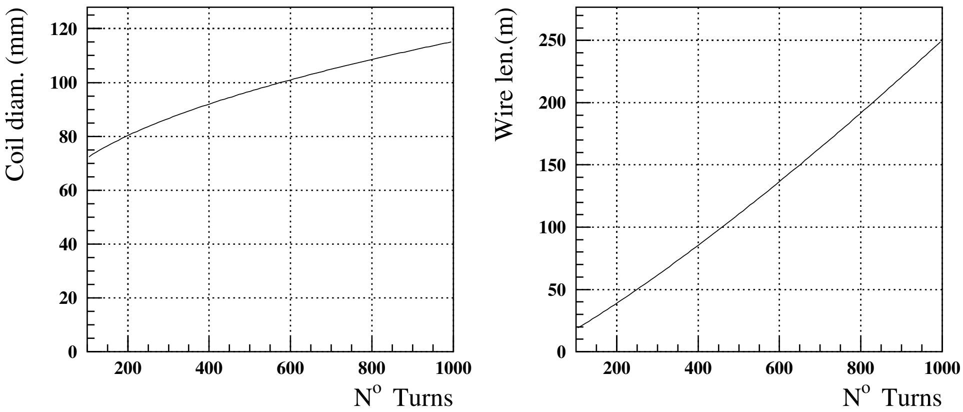

Figure 4: Overall diameter and wire length versus N. The choice $N = 400$ fixes $D = 92\ mm$ and $L = 85.5\ m$.

Finally we can estimate a "constant force region", or a trust zone, for z and ρ misalignments, by numerical integration of the equations describing the force contributions given by a segment of circular conductor, on a magnet at distance $\vec{r}(z,\rho)$. In Figure (5) we plotted the two force components, given by our coil/magnet, for various lateral misalignments.

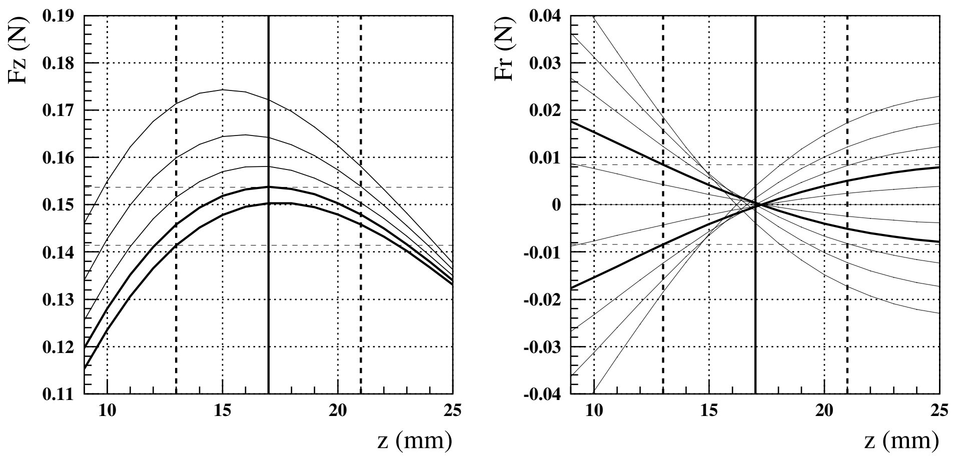

Figure 5: Behavior of the forces produced by our real coil with the $V = 942\ mm^3$ ($mz = 0.75\ Am^2$) magnet. Bold-face lines are referred to radial shift $r = \pm 4\ mm$, normal lines to greater radial shifts.

Within a zone of $4\ mm$ around the right point $(z_0, r_0) = (17, 0)$, the maximum force variation is:

$$0.1414 \leq F_z \leq 0.1537\ N$$
$$-0.0084 \leq F_r \leq +0.0084\ N$$

The radial force appearing when $r \neq 0$ and $z \neq z_0$ introduce a coupling between the degrees of freedom. In the trust zone $\Delta z, \Delta\rho = 4\ mm$, this coupling is at maximum of 6%. Moreover, its average over longitudinal and radial magnet dimension, would still low this value, due to the symmetry of the radial force respect to the point z_0, as shown in Fig. (5).

5.3 Coils characteristics

Here we summarize the coil's parameters, as deduced from the previous section:

- Number of turns: $N = 400$
- Current: $I = 1.12\ A$
- Mean Force/Current: 0.13 N/A
- Mean radius: $a = 34\ mm$
- Internal diameter (free): 42 mm
- Internal diameter (winding): 48 mm
- External diameter (winding): 88 mm
- Overall diameter: 92 mm
- Winding Cross Section: $S = 20\ mm \times 20\ mm$
- Conductor wire diameter : $d = 0.90\ mm$
- Insulated wire diameter (max): $d = 1.05\ mm$

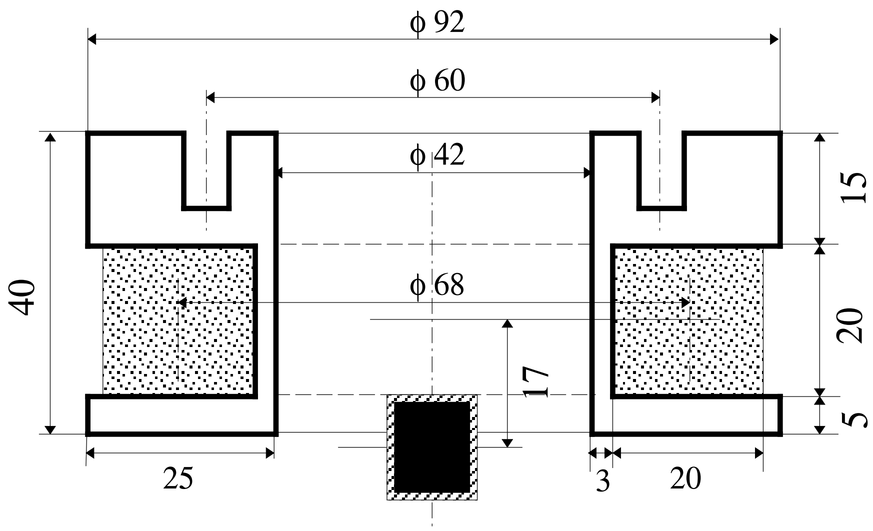

Figure 6: Coil and magnet in scale 1:1. The sprocket is constructed in Anticorodal 100 (Aluminum)

With these values we have a coil resistance of:

$$R = \frac{N\rho_{cu}2\pi a}{\pi r^2} = 2.44\ \Omega \quad (@300\ K) \tag{24}$$

and the fixed maximum dissipation of:

$$P_{max} = R \times I_{max}^2 = 3\ W \tag{25}$$

5.4 Magnets

Putting the magnet on the axis, at $z = a/2 = 17\ mm$ from the coil plane and with the overmentioned value of N,a and I, we need a permanent magnet of at least $m_{z_{min}} = 0.75\ Am^2$ to reach the mean force $\overline{F_z} = 0.146\ N$ of Figure (2).
The measure of the internal magnetic field B_r of a long ($\gg$ diameter) pillar of magnets gives us the value of the volume magnetic polarization (depending only on the material). Integrating it on one magnet volume, it gives :

$$m_z \times \mu_0 = B_r \times V$$

Samarium cobalt (SmCo2:17) magnets has been successfully tested for what concerned the outgassing rate and composition (VACPISA 047 P). In the table below we consider three hypothesis about the volume of such cylindrical magnets (options get from the Magnet Developments catalog). In our calculuses we have always used the first one ($m_z = 0.75\ Am^2$).

$N°$	$Dim\ (mm)$	$V_{tot}\ (mm^3)$	$B_r\ (T)$	$m_z\ (Am^2)$	$F/I\ (N/A)$
1	$d = 10;\ l_z = 12$	942	1	0.75	0.135
1	$d = 9.0;\ l_z = 15$	954	1	0.76	0.136
1	$d = 12.5;\ l_z = 10$	1227	1	0.98	0.175

5.5 Heat transfer

Heat removing in objects at room temperature and under vacuum occurs only through conduction. The radiative losses of our supports surface become important only if its temperature exceeds $\sim 400\ K$:

$$P_{irr} = 2.8 \cdot 10^{-9} \times (T - 300)^4\ W \tag{26}$$

We evaluated the heat conduction in steady-state by applying the Fourier's law

$$\vec{q} = -kA\vec{\Delta T} \tag{27}$$

in a two dimensional geometry. Like in one dimension, eq. (27) may be rewritten

$$q = -\frac{\Delta T}{R_{th}} \tag{28}$$

The proportional constant is referred to as the thermal resistance, which in one dimension depends on the distance L and on the dissipating surface A as $R_{th} = L/kA$, while in more than one is $R_{th} = 1/kS$, with S shape factor and k thermal conductivity.
The whole structure thermal resistance is a sum of several factors:

- Heat flow resistance from coil to its bracket (in two dimension geometry);
- About 55 mm of aluminum plates;
- Several contact resistances;
- A leg of length 58 cm, worked in aluminum or stainless steel with an H profile of 5 mm thickness .

The contribution of the first three is negligible respect to the fourth. Taking 204 $W/m°C$ as the aluminum thermal conductivity, the contribution of the first three terms is ~ 0.06 $°C/W$, against a leg thermal resistance of 1.5 $°C/W$ if made of aluminum, and ~ 21 $°C/W$ if made of stainless steel ($k = 15$ $W/m°C$).
We can calculate the coil temperature rise from (28). With two coils dissipating 3 W each, and the thermal resistance of a stainless steel leg of 21 $°C/W$, the temperature would increase of 126 $°C$, while, with an aluminum leg its rise would be only of 9 $°C$. These numbers blind us to use aluminum for the whole structure.

6 Transfered Noise

We transfer noise to the bench in two ways:

1. Through the voltage noise produced by the driver;
2. Through the seismic vibrations of the coils support.

6.1 Voltage noise

We can evaluate the first contribution considering a noise voltage v_n at the output of the driver. The model we will use has a maximum one of $v_n = 30\ nV/\sqrt{Hz}$, independent from the frequency, obtained with the gain factor at its maximum ($G = 10$); it supplies a maximum current of ~ 4 A. The tension v_n produces a current $i_n = v_n/R_{coil} = 12.3\ \ nA/\sqrt{Hz}$ and then a noise force, with white spectral density:

$$\widetilde{\Delta F} = 0.13 \times i_n = 1.6 \times 10^{-9} \quad \left[\frac{N}{\sqrt{Hz}}\right] \tag{29}$$

This force drives a noise, that at high frequency (above the resonances) has the following form :

$$\sqrt{< x^2(\nu) >_{volt.}} = \frac{4 \times \widetilde{\Delta F}}{M 4\pi^2\nu^2} \quad \left[\frac{m}{\sqrt{Hz}}\right] \tag{30}$$

$$\sqrt{< y^2(\nu) >_{volt.}} = \frac{2\sqrt{2} \times \widetilde{\Delta F}}{M 4\pi^2\nu^2} \quad \left[\frac{m}{\sqrt{Hz}}\right] \tag{31}$$

$$\sqrt{< \theta^2(\nu) >_{volt.}} = \frac{4 \times \widetilde{\Delta F} \times R_t}{I_{yz} 4\pi^2\nu^2} \quad \left[\frac{rad}{\sqrt{Hz}}\right] \tag{32}$$

$$\sqrt{< \phi^2(\nu) >_{volt.}} = \frac{4 \times \widetilde{\Delta F} \times R_r}{I_x 4\pi^2\nu^2} \quad \left[\frac{rad}{\sqrt{Hz}}\right] \tag{33}$$

with M and $I_{x,yz}$, mass and inertia moments of the bench only.
The calculated values are reported in the table at the end of this chapter.

6.2 Seismic noise

As regards the transfer of seismic noise, it's principally due to the error we made putting the magnet in the right position. Developing at the first order the (19) in a little space ϵ around the point $b = a/2 + \delta a$, we find:

$$\frac{\Delta F(b,\epsilon)}{F(b)} = \epsilon \left(\frac{5b}{(a^2+b^2)} - \frac{1}{b}\right) + O(\epsilon^2) \tag{34}$$

while the same expression vanishes near $a/2$ (non-zero terms only from the second order).
Supposing we are not be able to do better then $\delta a = 4\ mm$, and meaning with ϵ the power spectrum of the seismic noise (1), we will have:

$$\widetilde{\Delta F}(\nu) = \frac{2.76}{\nu^2} \cdot 10^{-6} \quad \left[\frac{N}{\sqrt{Hz}}\right] \tag{35}$$

The transfer, at high frequency, has the form of eq. (30). For the vertical mode it will be:

$$\sqrt{< x^2(\nu) >_{seis.}} = \frac{4 \times \widetilde{\Delta F}(\nu)}{M 4\pi^2 \nu^2} = \frac{4.66 \cdot 10^{-9}}{\nu^4} \times \left(\frac{60\ kg}{M}\right) \quad \left[\frac{m}{\sqrt{Hz}}\right] \tag{36}$$

and so on for the other modes.
In the two tables below are summed up the contribution of the noise sources (29) and (35) confronted with the limits given by the section 2.2:

@10 Hz	$\tilde{x_v}$ $\left[\frac{m}{\sqrt{Hz}}\right]$	$\tilde{y_h}$ $\left[\frac{m}{\sqrt{Hz}}\right]$	$\tilde{\theta}_t$ $\left[\frac{rad}{\sqrt{Hz}}\right]$	$\tilde{\phi}_r$ $\left[\frac{rad}{\sqrt{Hz}}\right]$
Seismic	$4.7 \cdot 10^{-13}$	$3.3 \cdot 10^{-13}$	$2.3 \cdot 10^{-12}$	$2.1 \cdot 10^{-12}$
Voltage	$2.8 \cdot 10^{-14}$	$2.0 \cdot 10^{-14}$	$1.4 \cdot 10^{-13}$	$1.3 \cdot 10^{-13}$
Limits	10^{-8}	10^{-8}	1.44×10^{-8}	1.44×10^{-8}

@100 Hz	$\tilde{x_v}$ $[\frac{m}{\sqrt{Hz}}]$	$\tilde{y_h}$ $[\frac{m}{\sqrt{Hz}}]$	$\tilde{\theta}_t$ $[\frac{rad}{\sqrt{Hz}}]$	$\tilde{\phi}_r$ $[\frac{rad}{\sqrt{Hz}}]$
Seismic	$4.7 \cdot 10^{-17}$	$3.3 \cdot 10^{-17}$	$2.3 \cdot 10^{-16}$	$2.1 \cdot 10^{-16}$
Voltage	$2.8 \cdot 10^{-16}$	$2.0 \cdot 10^{-16}$	$1.4 \cdot 10^{-15}$	$1.3 \cdot 10^{-15}$
Limits	10^{-10}	10^{-10}	1.44×10^{-8}	1.44×10^{-8}

7 Damping

According to the Introduction, the other goal of our system is to control and damp the bench oscillations at the resonant frequencies.
By applying a force proportional to the velocity $F(t) = \beta v(t)$, one performs a viscous damping.
We would a critical Quality Factor $Q \leq 1$ for all modes, to control the bench movements without oscillations, during its displacements. From this condition we deduce a viscous coefficient $\beta = 2M\omega_{ris}$ ($2I\omega_{ris}$ for rotational modes).
Solving the equation describing the motion of a damped pendulum, we obtain that the maximum initial amplitude one can damp is linked to the maximum force performed as:

$$A_{max}(0) = \frac{F_{max} \cdot e}{2M\omega_r^2} \tag{37}$$

with e Nepero's number.
If $A(0)$ is greater than this, the bench would make some oscillations before stop (i.e a quality factor $Q > 1$).
Below we list the maximum amplitude (37), calculated for all the controlled modes.

- Vertical: $A_{max}(0) = 2.3\ mm$
- Horizontal: $A_{max}(0) = 3.3\ mm$
- Tilt: $A_{max}(0) = 32 \cdot 10^{-3}\ rad$
- Rotation: $A_{max}(0) = 3.2\ rad$

8 Geometrical disposition and design considerations

The idea is to attach four legs to the tower floor and to mount two coils each, one horizontal and one vertical, faced from the respective magnets. In such a way we have four vertical actuators, controlling three degrees of freedom, and other horizontal four controlling the other three degrees, having so the redundancy of one, in case (even if remote) of breaking during working operations. Figure (8) shows a bench scaled scheme.
The magnets faced to the coils controlling the vertical modes are attached under the bench. The "horizontal" magnets are attached on a bracket as rigid as possible, on the bench side. Every magnet can be moved along its axis by a threaded covering, in order to put it at the right distance from the coil.
The coil's mounting allows horizontal movements in two directions by shifting the superposed plates, and vertical movements through plates of different thickness. The distance between the two coils mounted on the same leg is fixed, as is fixed the distance between the respective magnets on the bench.
On each leg is also present a vertical pivot, screwed on one plate, that will be used to lay the bench and make some initial tests.

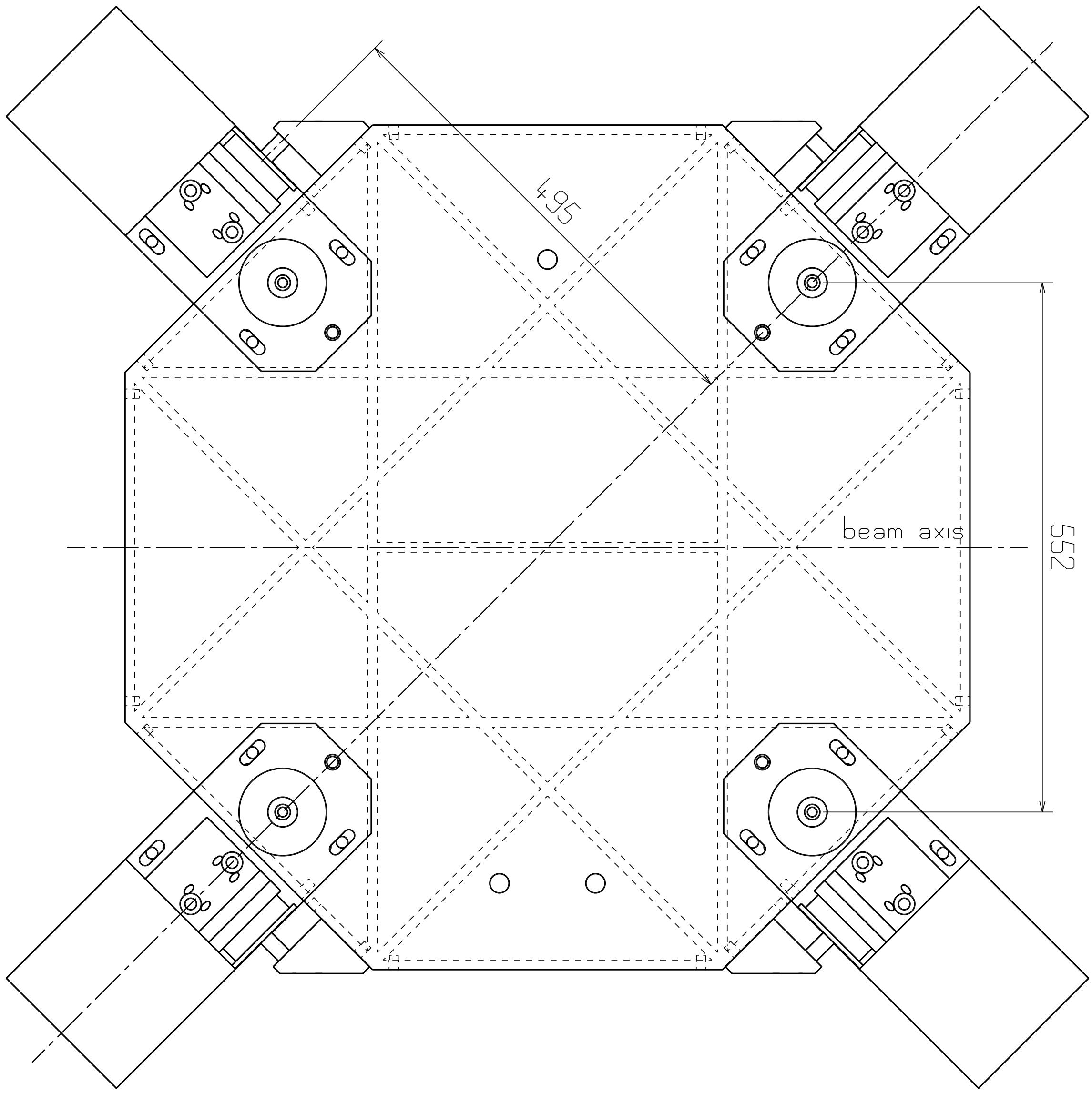

Figure 7: Detection Bench plan. Are indicated the couple's arms, applied to perform rotations and tilts.

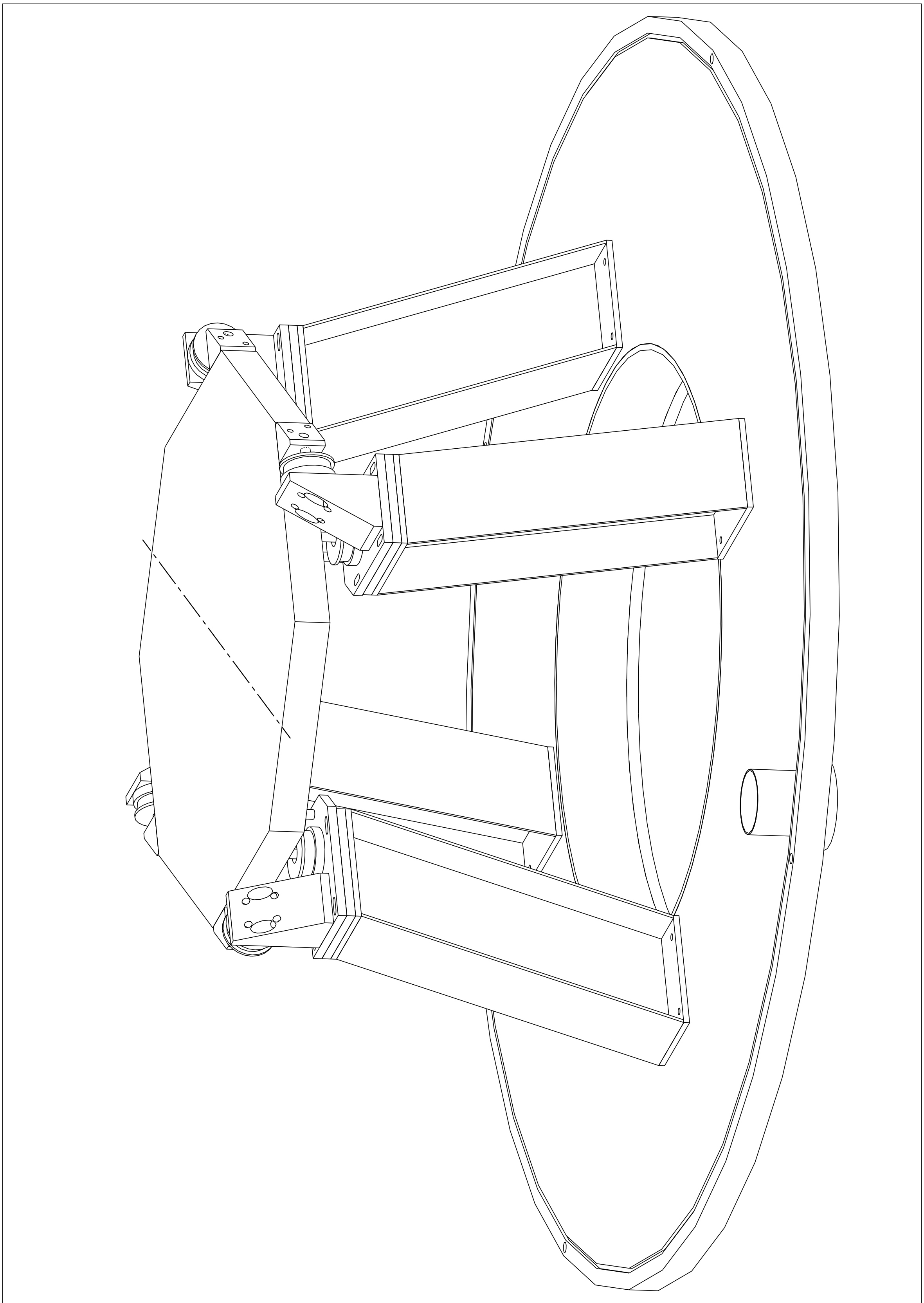

Figure 8: A scaled scheme of the detection bench with the coil's legs mounted on the tower floor.